IJNAOE
©SNAK, 2014

Int. J. Nav. Archit. Ocean Eng. (2014) 6:119~131
http://dx.doi.org/10.2478/IJNAOE-2013-0167
pISSN: 2092-6782, eISSN: 2092-6790

Influence of the empirical coefficients of cavitation model on predicting cavitating flow in the centrifugal pump

Hou-lin Liu, Jian Wang, Yong Wang, Hua Zhang and Haoqin Huang

Research Center of Fluid Machinery Engineering and Technology, Jiangsu University, Zhenjiang, China

ABSTRACT: *The phenomenon of cavitation is an unsteady flow, which is nearly inevitable in pump. It would degrade the pump performance, produce vibration and noise and even damage the pump. Hence, to improve accuracy of the numerical prediction of the pump cavitation performance is much desirable. In the present work, a homogenous model, the Zwart-Gerber-Belamri cavitation model, is considered to investigate the influence of the empirical coefficients on predicting the pump cavitation performance, concerning a centrifugal pump. Three coefficients are analyzed, namely the nucleation site radius, evaporation and condensation coefficients. Also, the experiments are carried out to validate the numerical simulations. The results indicate that, to get a precise prediction, the approaches of declining the initial bubble radius, the condensation coefficient or increasing the evaporation coefficient are all feasible, especially for declining the condensation coefficient, which is the most effective way.*

KEY WORDS: Cavitation flow; Centrifugal pump; Experiment; Numerical simulation.

INTRODUCTION

The occurrence of unsteady cavitation in pump is nearly inevitable, where the local pressure drops below the saturated vapor pressure, especially for those applied on vessels and offshore platforms, since the particles contained in seawater can increase the probability of cavitation generation. Cavitation may cause various problems, like vibration, noise and material erosion, which would deteriorate the pump performance and cause damage to the pump (Brennen et al., 1995; Ding et al., 2011; Bruno and Frank, 2009). In the recent years, owing to the continuous improvement of Computational Fluid Dynamics (CFD) technologies and computational capabilities, the prediction of pump cavitation performance based on CFD method has been beneficial for preliminary pump design (Liu et al., 2010; 2012; Wang et al., 2011; Dijkers et al., 2005). Thus, it makes the cavitation model play a significant role in numerical simulation progress. During the last decades, great efforts have been made in the development of cavitation models (Athavale et al., 2002; Coutier-Delgosha et al., 2003). These models can be put into two categories, namely interface tracking methods (Senocak and Shyy, 2004; Hirschi et al., 1998) and homogeneous equilibrium flow models (Zwart et al., 2004; Kunz et al., 2000; Singhal et al., 2002; Schnerr and Sauer, 2001; Merkle et al., 1998; Delannoy and Kueny, 1990). The former assumes that the cavity region has a constant pressure equal to the vapor pressure of the corresponding liquid and the computations are calculated only for the liquid phase. However, these methods are limited to 2-D planar or axisymmetric flows because of the difficulties dealing with complicated 3-D models. In the second category, the homogeneous equilibrium flow models assume the flow to be homogenous and isothermal, applying either a barotropic

Corresponding author: *Jian Wang*, e-mail: *arieskin@126.com*

equation of state or a transport equation for both phases. The barotropic equation links the density to the local static pressure (Delannoy and Kueny, 1990). A recent experimental study implied that the vorticity production is an important aspect of cavitating flows, especially in the cavity closure region (Gopalan and Katz, 2000). But in the barotropic law, the gradients of density and pressure are always parallel, which leads to zero baroclinic torque. Therefore, the barotropic cavitation models cannot capture the dynamics of cavitating flows, particularly for cases with unsteady cavitation flows (Senocak and Shyy, 2002). Furthermore, this method is prone to instability because of high pressure-density dependence, which makes it difficult to reach the convergence levels of noncavitating flow simulations (Marina, 2008). Conversely, these limitations can be avoided by applying the transport equation models (TEM). In this approach, volume or mass fraction of the two phases are solved by an additional transport equation with different source terms. Besides, there is another apparent advantage of this method, which could predict the impact of inertial forces on cavities like elongation, detachment and drift of bubbles. In the past years, a great number of transport equation models are proposed (Zwart et al., 2004; Kunz et al., 2000; Singhal et al., 2002; Schnerr and Sauer, 2001; Merkle et al., 1998). These models apply different condensation and evaporation empirical coefficients to regulate the mass and momentum exchange. However, most of these empirical coefficients are calibrated on simple hydraulic machinery, such as hydrofoil or blunt body. When these models are employed in pumps, the accuracy of numerical simulation is strongly dependent on users' experience to choose proper coefficients. Among this kind of TEM models, because of its effectively and stability, the Zwart-Gerber-Belamri model (hereafter ZGB model) was widely used for different cases (Zwart et al., 2004; Hagar et al., 2012; Liu et al., 2012).

In this study, the influence of the empirical coefficients on predicting the cavitation performance of a centrifugal pump was investigated. To this aim, the ZGB model was considered. Moreover, the experiments were carried out to validate the numerical simulations.

EXPERIMENTAL SETUP AND TEST PUMP

The experiments were performed on a closed platform in the Research Center of Fluid Machinery Engineering and Technical of Jiangsu University. Fig. 1 shows the centrifugal pump closed test rig. Two pressure transducers, JYB-KO-HAG-L-1, are installed in the upper and down steam, with a measurement accuracy of ±0.5%FS (The FS is interpreted as the full scale of the pressure transducer, which is ±100*kPa*). To avoid the disturbance from the pump, a turbine flowmeter LWGY-80A is mounted far away from the pump, with an accuracy of ±0.5% for the flow-rate value between 16-100m^3/h. Measurement uncertainties were estimated to be less than ±2% and ±1.5% respectively, contributing to an uncertainty of ±2.8% of the pump head and ±2% of the cavitation number, according to Eqs. (9) and (11). All of the measured data are acquisitioned synchronously and then processed by a pump test system, TPA, developed by our research center. The ambient temperature is about 22° and after 3 times tests, the system is ceased for hours until the water temperature cools down.

Fig. 1 Experimental setup.

The basic parameters of the test pump are listed as follows: the volume flow rate $Q = 0.014 m^3/s$, the rotation speed $n =$ 2,900*r/min*, the impeller diameter $D_2 = 168mm$ and the blade number $Z = 5$. The impeller test model is given in Fig. 2(a), which is manufactured by the rapid prototyping technology. Its meridional shape is also plotted in Fig. 2(b).

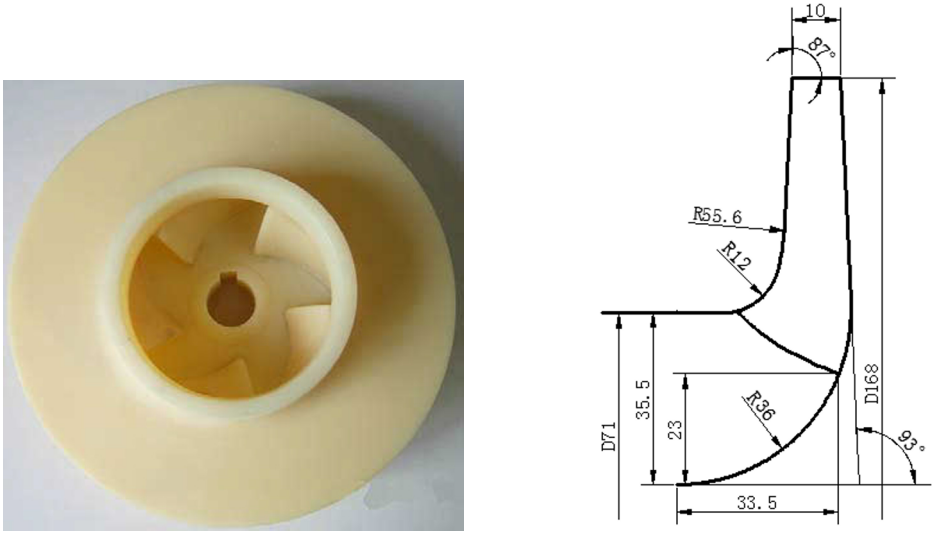

(a) (b)

Fig. 2 Test impeller model (a) and impeller meridional shape (b).

NUMERICAL SIMULATION METHOD

Governing equations

The set of governing equation consists of the mass continuity (1) and momentum Eq. (2) plus a transport Eq. (3) to define vapor generation:

$$\frac{\partial \rho_m}{\partial t} + \frac{\partial}{\partial x_i}(\rho_m \overline{u_i}) = 0 \tag{1}$$

$$\frac{\partial(\rho_m \overline{u_i})}{\partial t} + \frac{\partial(\rho_m \overline{u_i}\overline{u_j})}{\partial x_i} = -\frac{\partial p}{\partial x_i} + \frac{\partial}{\partial x_j}\left[(\mu_m + \mu_t)\left(\frac{\partial \overline{u_i}}{\partial x_j} + \frac{\partial \overline{u_j}}{\partial x_i} - \frac{2}{3}\delta_{ij}\frac{\partial \overline{u_k}}{\partial x_k}\right)\right] \tag{2}$$

$$\frac{\partial \alpha_v}{\partial t} + \frac{\partial(\alpha_v \overline{u_i})}{\partial x_i} = \dot{m}^+ + \dot{m}^- \tag{3}$$

The mixture density is defined by the vapor volume fraction, expressed as:

$$\rho_m = \rho_v \alpha_v + \rho_l (1 - \alpha_v) \tag{4}$$

where p is the pressure, ρ_m is the mixture density, u_i is the velocity, μ and μ_t stand for the laminar viscosity and turbulent viscosity, α is the volume fraction, $\dot{m}^+$ and $\dot{m}^-$ represent the source terms for evaporation and condensation. The subscripts *m*, *l*, *v* indicate the mixture, liquid and vapor, respectively.

Turbulence model

The RNG *k-ε* model was adopted for solving the transport equations of the turbulent kinetic energy and its dissipation rate, which is based on the renormalization group analysis of the Navier-Stokes equations. The RNG *k-ε* model has been proved to give good predictions in cavitating flows (Zhou and Wang, 2008; Chang and Wang, 2012; Yang et al., 2012). To improve the numerical simulations, a modification of the turbulent viscosity was taken into account to reduce the turbulent viscosity of the mixture, proposed by Coutier-Delgosha et al., (2003). The turbulent viscosity μ_t is defined as

$$\mu_t = f(\rho_m) C_\mu \frac{k^2}{\varepsilon} \tag{5}$$

$$f(\rho_m) = \rho_v + \frac{(\rho_m - \rho_v)^n}{(\rho_l - \rho_v)^{n-1}} \tag{6}$$

where the exponent n is a constant and Fig. 3 shows the relationship between different n values with $f(\rho_m)$. It can be noted that, with increasing n, the turbulence viscosity would reduce obviously. As recommended by Coutier-Delgosha et al., (2003), $n = 10$ was employed in the present study.

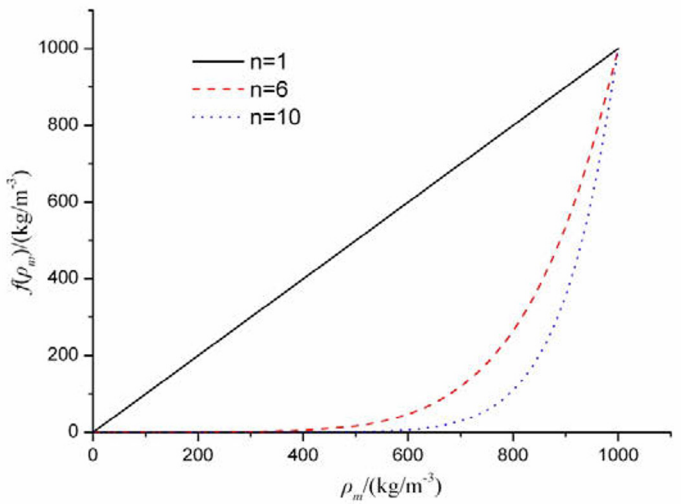

Fig. 3 Relationship between function $f(\rho_m)$ and mixture density ρ_m with different n values.

Cavitation model

All the simulations were conducted by using the ANSYS-CFX commercial software and the ZGB model was considered in this paper, which is deduced from the Rayleigh-Plesset equation:

$$\dot{m}^+ = F_{vap} \frac{3 r_{nuc}(1-\alpha_v)\rho_v}{R_B} \sqrt{\frac{2}{3}\frac{p_v - p}{\rho_l}}, \text{ if } p<p_v \tag{7}$$

$$\dot{m}^- = F_{cond} \frac{3 \alpha_v \rho_v}{R_B} \sqrt{\frac{2}{3}\frac{p - p_v}{\rho_l}}, \text{ if } p>p_v \tag{8}$$

where F_{vap} and F_{cond} are the empirical calibration coefficients of evaporation and condensation, respectively. And r_{nuc} is the nucleation site volume fraction, R_B stands for the nucleation site radius (hereafter NSR). Vaporization is initiated at nucleation

sites, which can be regarding as the non-condensible gases. p_v represents the water vaporization pressure. The recommended values of these coefficients are: $F_{vap}=50$, $F_{cond}=0.01$, $r_{nuc}=5\times10^{-4}$, $R_B=2\times10^{-6}m$ and $p_v=3574Pa$. In this paper, the coefficients, F_{vap}, F_{cond} and R_B, were studied to find out the influence on predicting the cavitating flows in centrifugal pump.

Meshing

To get a good accuracy computing results, the structured hexahedral grids were generated by GridPro commercial software. Fig. 4(a) shows the computational fluid domain of the centrifugal pump. The grids near the blade surface region layer were refined, which is locally zoomed up in Fig. 4(b). The Y plus on the blade surface is ranged from 0.2 to 35 (Fig. 5). To get a relatively stable upper and down stream flow, two prolongations, whose lengths are four times of the pipe diameter, were assembled on the impeller and volute.

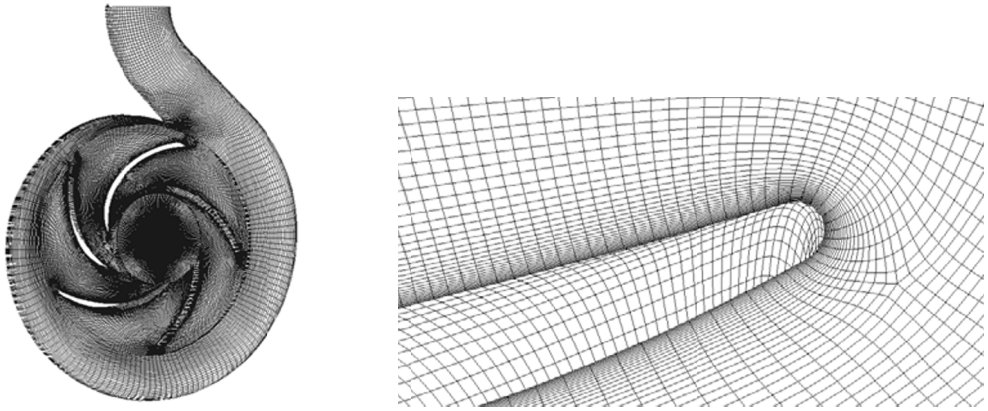

(a) (b)

Fig. 4 Pump computational grids (a) and grid refinement on blade (b).

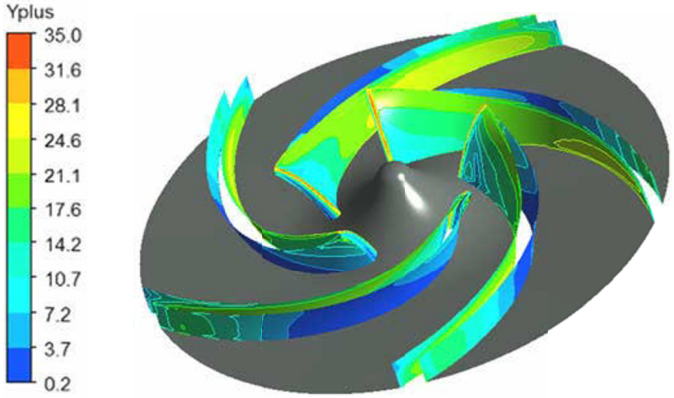

Fig. 5 Yplus on the blade surface.

A mesh independence test was performed based on the pump head H under non-cavitation condition, calculated by Eq. (9).

$$H=\frac{\left(p_{tout}-p_{tin}\right)}{\rho g} \tag{9}$$

where p_{tin} and Pp_{tout} represent the total pressure of the inlet and outlet, respectively.

Table 1 gives the simulation results with five different kinds of grid density. It is obviously that when the cell number is over two million, the discrepancy of the pump head is within 1%. Ultimately, considering the simulation efficiency, the total cell number of all the domains are set as 1.20×10^6.

Table 1 Pump head with different cell numbers.

	Cell number/10^6	Pump head/m
1	0.62	31.54
2	1.20	30.86
3	1.81	30.74
4	2.57	30.74

Boundary condition

In the simulation process, since the pump impeller is a rotating part, whereas the other parts, the prolongations and volute casing, are stators, the Multiple Reference Frame (MRF) approach was employed, which allows the analysis of situations involving rotator/stator fluid domains and has been demonstrated that it has good accuracy (Ding et al., 2011; Lei et al., 2012). The interfaces were imposed between the impeller and inlet prolongation and volute. The pressure and mass flow rate boundary conditions were fixed at the inlet and outlet, respectively. Moreover, no slip boundary condition was applied on the solid surface of the pump. All the calculations were firstly carried out under non-cavitation condition to obtain a steady solution. Then, the pressure loaded on the inlet was decreased progressively until the desired cavitation number was reached.

RESULTS AND DISCUSSIONS

In the convenience of comparing the results, two dimensionless parameters are defined as:

$$\text{Pump head coefficient} \quad \psi = H \Big/ \left(u_2^2/2g\right) \tag{10}$$

$$\text{Cavitation number} \quad \sigma = \left(p_{in} - p_v\right) \Big/ 0.5\rho_l u_2^2 \tag{11}$$

where u_2 is the circumferential velocity at the impeller outlet, p_{in} represents the static pressure of the inlet.

Influence of the nucleation site radius

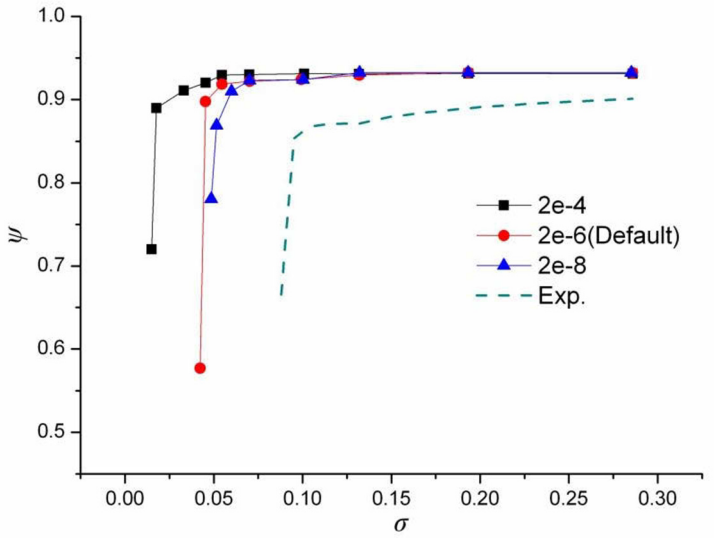

Fig. 6 Influence of the NSR on pump head drop curve.

In Fig. 6, the pump head drop characteristic curves are shown, calculated by different NSR, while the other empirical coefficients are set as default. To distinguish the experimental results from the numerical simulations, the experimental results are plotted as dash line, whereas the straight lines with symbols stand for the computed results. Apparently, the smaller NSR, such as $R_B = 2 \times 10^{-8} m$, the closer the results to the experiment. Under non-cavitation conditions, compared with the experiment, a slight overestimation of the pump head can be observed in simulations. Here we define a scaleless parameter-the critical cavitation number σ_c as the σ value when the pump head drops by 3%. The σ_c values of each conditions are 0.027, 0.048 and 0.059, successively from $R_B = 2 \times 10^{-4} m$ to $2 \times 10^{-8} m$, whereas the value in the experiment is 0.138, almost three times larger than $R_B = 2 \times 10^{-6} m$ (default).

In Fig. 7, the vapor volume fraction distribution with various R_B when $\sigma = 0.07$ at Span = 0.5 are plotted. The Span is defined as the dimensionless distance (0-1) from the hub to shroud. It's important to note the rotating direction is from bottom to top and the flow direction is from left to right. As seen, great discrepancy can be observed. When $R_B = 2 \times 10^{-6} m$, the cavity region, where the vapor volume fraction is nearly 1.0, is attached on the suction side of the blade surface, and then the fraction gradually decreases in the normal direction. However, as R_B rising to $2 \times 10^{-4} m$, there are only a few bubbles with very low volume fraction (Notice that the legends are different from the others). In the opposite case, when R_B reduces to $2 \times 10^{-8} m$, the cavity region is approximately identical with the case of $R_B = 2 \times 10^{-6} m$, except for the high vapor volume fraction area. In the case of $R_B = 2 \times 10^{-8} m$, the cavity region with high fraction is much larger than the others, contributing to producing a larger low pressure region on the blade surface. This can be observed in Fig. 8, which presents the blade loading distribution on the middle streamline at Span = 0.5 when $\sigma = 0.07$. The horizontal axis, streamwise, stands for a streamwise coordinate that follows the blade surface and it ranges from 0 at the leading edge to 1 at the trailing edge of the blade. The vertical axis represents the pressure loading on the blade surface. All the data are computed from the blades zoomed up in Fig. 7(d).

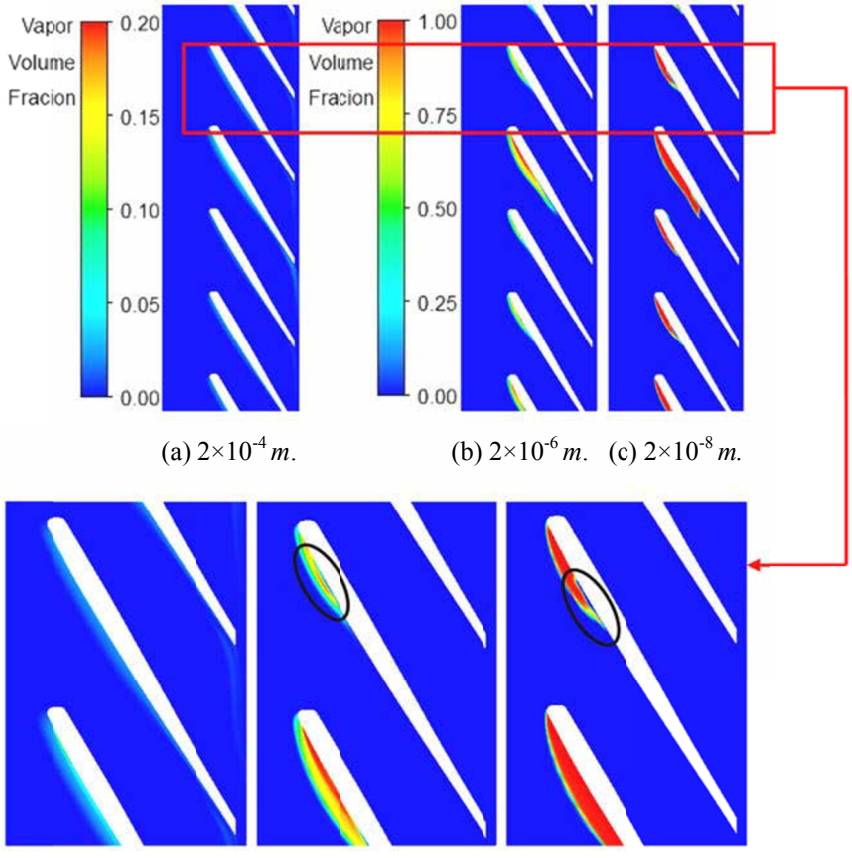

(a) $2 \times 10^{-4} m$. (b) $2 \times 10^{-6} m$. (c) $2 \times 10^{-8} m$.

(d) blades zoom in.

Fig. 7 Vapor volume fraction distribution with various NSR when $\sigma = 0.07$ at Span = 0.5.

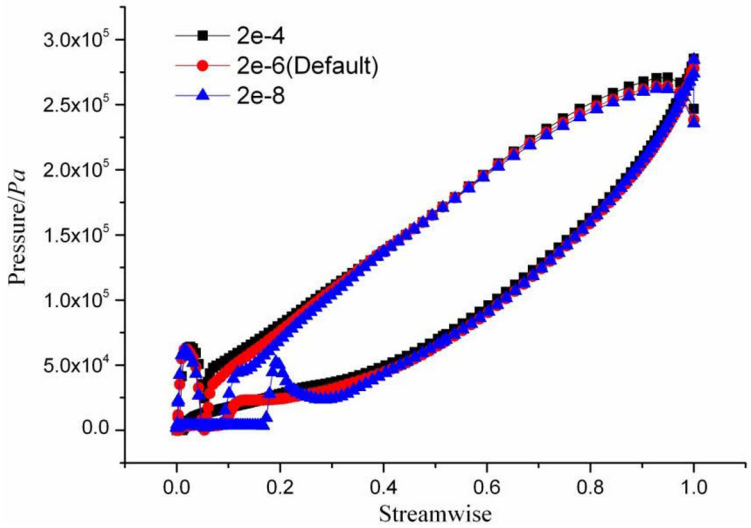

Fig. 8 Blade loading distribution with various NSR on the middle streamline at Span = 0.5.

In Fig. 8, the upper curves are the data of the pressure side, while the below ones are the suction side. We can find that the pressure loading distributions on both sides of the blade are almost similar under different NSR, except for the leading edge of the suction side. For the case of higher NSR, the pressure on the suction side gradually rises from the leading edge to the trailing edge. It is mainly because there are a few bubbles with low volume fraction attached on the blade surface (Fig. 7(d)). The situation becomes different when the NSR drops. Due to the bubbles with high vapor volume fraction attached on the leading edge of the suction side, the pressure on this place are approximately zero and the length of the low pressure region increases with the decreasing NSR. For $R_B = 2 \times 10^{-8} m$, the length is around 0.18, compared with the case of $R_B = 2 \times 10^{-6} m$, whose low pressure region length is about 0.1. Meanwhile, it is interesting to see that the pressure gets a sharply increase just after the low pressure region and then it has a slightly decline, which is much more obvious when $R_B = 2 \times 10^{-8} m$. The reason lies in the fact that the re-entrant jet in the cavity region near the blade surface, keeps the bubbles away from the blade, which is emphasized in Fig. 7(d) by black ellipses. And as the detached cavity gets close to the blade surface, the pressure drops a little bit and then soars again. Besides, on the pressures side of the leading edge, a humped curve is also observed of all the cases, which is probably caused by the high curvature, leading to flow separation at that point.

Influence of the evaporation and condensation coefficients

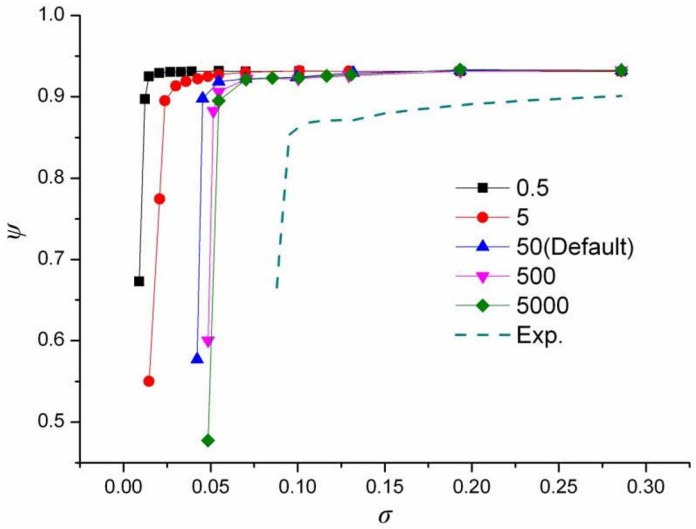

Fig. 9 Influence of the evaporation coefficient on pump head drop curve.

Since the evaporation and condensation coefficients have much more influence on the calculation, more schemes are chosen. The results are given in Fig. 9. As seeing, the smaller F_{vap} value, the greater discrepancy between the numerical simulation and the experiment. It can be observed that when F_{vap}<50(default value), the pump head starts to drop at a very low cavitation number. For F_{vap} = 5, the critical cavitation number σ_c = 0.027 and for F_{vap} = 0.5, this value drops to 0.013. It is implied that reducing the F_{vap} value would greatly impact the computed result. In contrast, when increasing the evaporation coefficient, a slightly improvement of the head drop curve can be noticed. But compared with the experiment result, σ_c = 0.138, the critical cavitation number only goes up to 0.054 and 0.06, respectively for F_{vap} = 500 and F_{vap} = 5000.

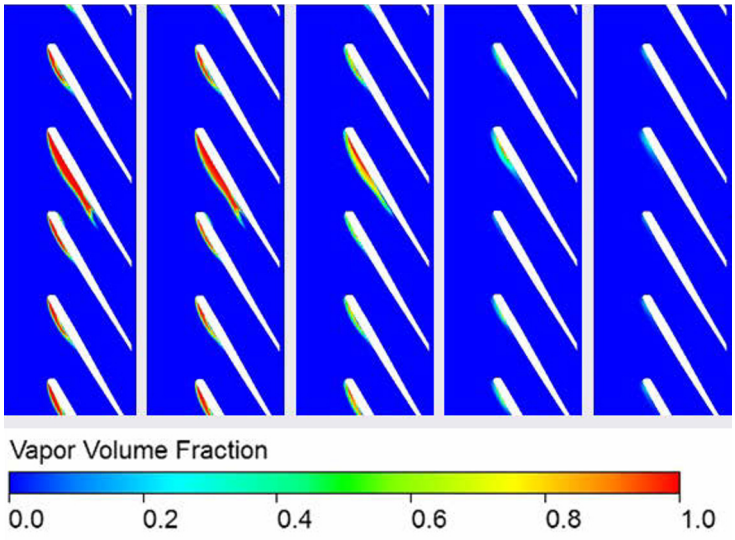

(a) F_{vap} = 5000. (b) F_{vap} = 500. (c) F_{vap} = 50. (d) F_{vap} = 5. (e) F_{vap} = 0.5.

Fig. 10 Vapor volume fraction distribution with various evaporation coefficients when σ = 0.07 at Span = 0.5.

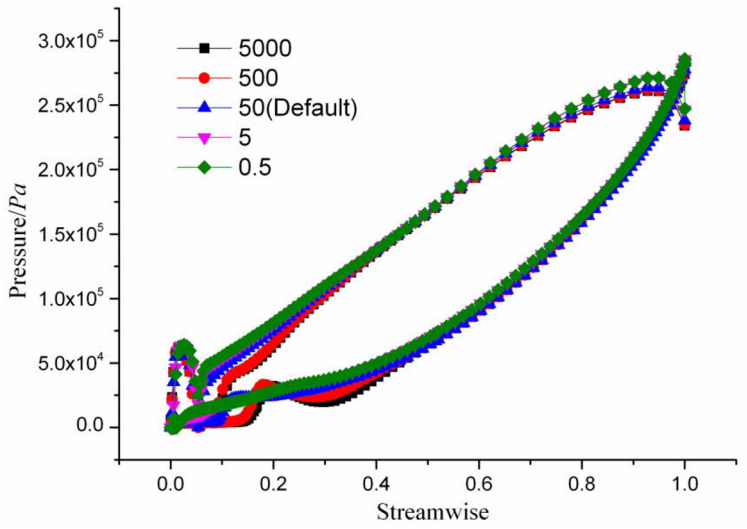

Fig. 11 Blade loading distribution with various evaporation coefficients on the middle streamline at Span=0.5.

Figs. 10 and 11 present the vapor volume fraction distribution and blade loading distribution with various evaporation coefficients under the same conditions as Figs. 7 and 8. From Fig. 10, it can be find out that both of the cavity size and length are getting smaller and shorter as the evaporation coefficients declining, leading to diminishing the low blade loading region, as can be seen in Fig. 11. In addition, it is obviously that when the F_{vap} value increases, the cavity region with high vapor volume fraction become larger.

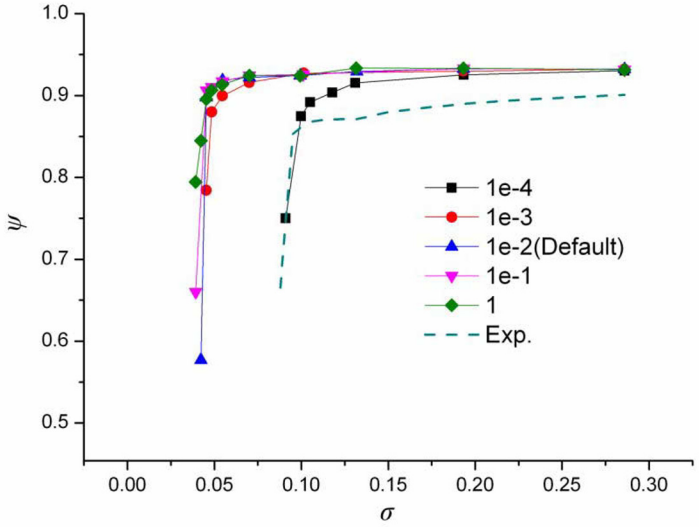

Fig. 12 Influence of the condensation coefficient on pump head drop curve.

Fig. 12 shows the head drop curves with different condensation coefficients. Similarly, five values are selected to investigate. We can see when increasing F_{cond} from 1e-2 to 1e-1 and 1, the head drop curve nearly has no change. The critical cavitation number σ_c are 0.047 and 0.045, respectively for F_{cond} = 1e-1 and 1, compared with σ_c = 0.048 as F_{cond} = 1e-2 (default value). While F_{cond} drops to 1e-3, a better prediction result is obtained. The pump head starts to decline when σ is around 0.07, contributing to a higher critical cavitation number σ_c = 0.059. But when the condensation coefficient F_{cond} reduces to 1e-4, a tremendous improvement can be noticed in the figure. The head drop curve has a good agreement the experiment, with a critical number σ_c of 0.116, compared with 0.138 in the experiment.

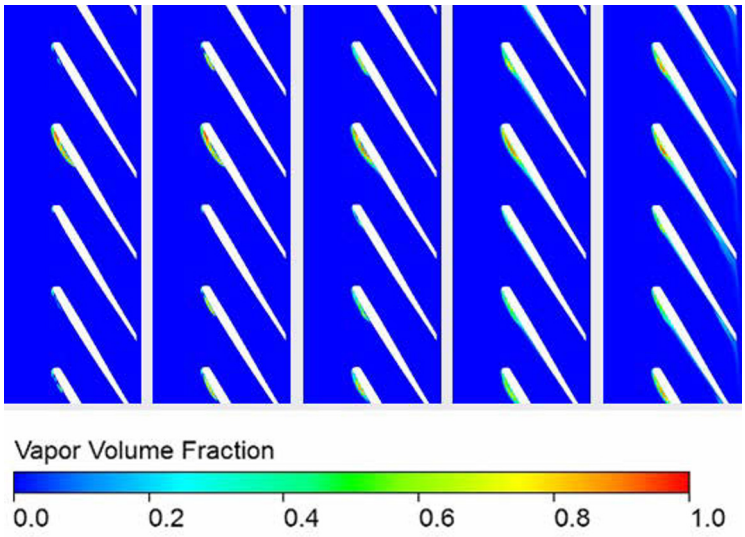

(a) F_{cond} = 1. (b) F_{cond} = 1e-1. (c) F_{cond} = 1e-2. (d) F_{cond} = 1e-3. (e) F_{cond} = 1e-4.

Fig. 13 Vapor volume fraction distribution with various condensation coefficients when σ = 0.1 at Span = 0.5.

Since the cavitation number in the case of F_{cond} = 1e-4 is higher than the others, the operating condition of σ = 0.1 is chosen to study the vapor volume fraction distribution, which is shown in Fig. 13. It is noticed that with the condensation coefficient dropping, the cavity length is getting longer. As F_{cond} = 1e-4, the bubbles nearly cover all over the suction side of the blade, which produces a more accuracy prediction results. The reason lies in that, with lower condensation coefficient, the mass of vapor transferred into liquid decreased, making the cavity length much longer. Furthermore, we can find that the cavity of high volume fraction is almost unchanged with decreasing F_{cond}. Also, the blade loading with various condensation coefficients are

plotted in Fig. 14. No remarkable difference can be observed, that is to say, the most affective factor for blade loading is the cavity region of high volume fraction, but not the cavity length.

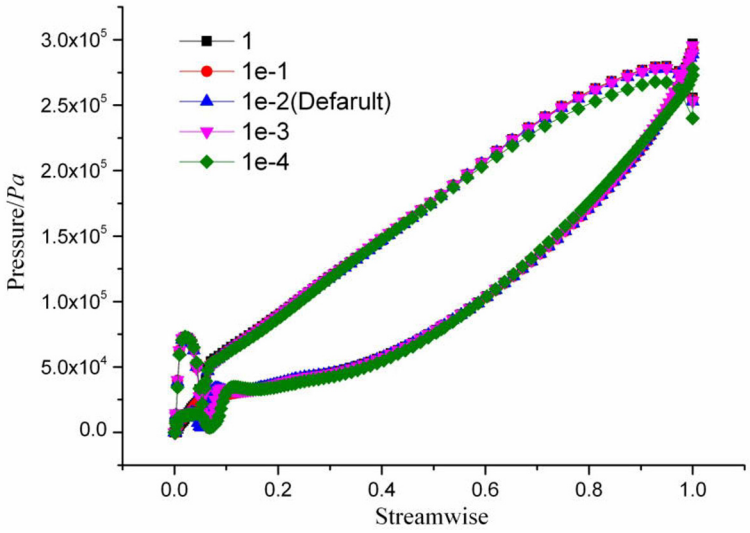

Fig. 14 Blade loading distribution with various condensation coefficients on the middle streamline at Span = 0.5.

CONCLUSIONS

To investigate the influence of the empirical coefficients of cavitation model on predicting cavitating flow in centrifugal pump, numerical simulation and experiment are presented in this paper. The widely used Zwart-Gerber-Belamri cavitation model is considered. Within this model, three coefficients are analyzed, namely the nucleation site radius R_B, evaporation and condensation coefficients, F_{vap} and F_{cond}. During the simulation process, when one of these coefficients is studied, the others are set as default. The conclusions could be arrived at as follows:

(1) The nucleation site radius is considered in the first place with three different values, R_B=$2\times10^{-4}m$, $2\times10^{-6}m$ and $2\times10^{-8}m$. Compared with the experiment, the computed results show that the accuracy of the predictions of the pump cavitation performance is improved as the NSR decreasing. Meanwhile, the vapor volume fraction distribution and the blade loading distribution under certain operation condition are analyzed. For smaller NSR, both of the cavity length and the cavity region of high volume fraction increase, which would promote to degrade the pump head. Besides, because of the re-entrant jet, the low pressure region on the leading edge of the suction side of the blade is much larger with small NSR.

(2) Then, the evaporation and condensation coefficients are researched. It can be noticed that, to obtain more precisely simulation results, one can either increases the evaporation coefficient or decreases the condensation coefficient. Moreover, it is important to note that the later approach has much more impact on the predictions than the former and produces progressively better results. To figure it out, the vapor volume fraction distribution is also studied. It is concluded that, the evaporation coefficient controls both the cavity length and the high vapor volume fraction cavity region, and the later factor is more affective on the pressure loading on the blade, but less effective on numerical predictions. On the other hand, the condensation coefficient mostly regulates the cavity length, while the high vapor volume fraction nearly remains identical. And it is observed that, when the cavity covers all over the suction side of the blade, the simulation result has the best agreement with the experiment. However, while the cavity length is within the blade, the simulation results have only a little change. Hence, comparing the influence of the evaporation and condensation coefficients, we may draw the conclusion that the cavity length is the most effect factor degrading the pump head. While the cavity region with high vapor volume fraction is the main factor which impacts the blade loading pressure greatly, but has little impact on the improvement of numerical predictions.

ACKNOWLEDGEMENTS

This research is funded by the National Natural Science Foundation of China (51309120, 51239005, 51109095, 51179075), the National Science & Technology Pillar Program of China (2011BAF14B03, 2013BAF01B02 and 2013BAK06B02), Natural Science Foundation of Jiangsu Province of China (BY2011140); Senior talents project funded Jiangsu university (12JDG 044); A Project Funded by the Priority Academic Program Development of Jiangsu Higher Education Institutions and Jiangsu Planned Projects for Postdoctoral Research Funds(1202076C); The Scientific Research Innovation Program in Colleges and Universities of Jiangsu Province (Grant No. 1293000468)

REFERENCES

Athavale, M.M., Li, H.Y., Jiang, Y.U. and Singhal, A.K., 2002. Application of the full cavitation model to pumps and inducers. *International Journal Rotating Machchinery*, 8(1), pp.45-56.

Brennen, C.E., 1995. *Cavitation and bubble dynamics, Oxford engineering & sciences series 44*. New York: Oxford University Press.

Chang, S.P. and Wang, Y.S., 2012. Cavitation performance research of mixed-flow pump based on CFD. *Journal of Drainage and Irrigation Machinery Engineering*, 30(2), pp.171-176.

Coutier-Delgosha, O., Hofmann, M., Stoffel, B., Fortes-Patella, R. and Reboud, J.L., 2003. Experimental and numerical studies *in* a centrifugal pump with two-dimensional curved blades in cavitating condition. *Journal of Fluids Engineering*, 125(6), pp.970-978.

Coutier-Delgosha, O., Fortes-Patella, R. and Reboud, J.L., 2003. Evaluation of the turbulence model influence on the numerical simulations of unsteady cavitation. *Journal of Fluids Engineering*, 125(1), pp.38-45.

Delannoy, Y. and Kueny, J.L., 1990. Two phase flow approach in unsteady cavitation modeling. *Cavitation and Multiphase Flow Forum, FED 98*, pp.153-158.

Dijkers, R.J.H., Fumex, B., de Woerd, J.O., Kruyt, N.P. and Hoeijmakers, H.W.M., 2005. Prediction of sheet cavitation in a centrifugal pump impeller with the three-dimensional potential-flow model. *ASME Fluids Engineering Division Summer Meeting and Exhibition*, Houston, USA, 19-23 June 2005, pp.1233-1238.

Ding, H., Visser, F.C., Jiang, Y. and Furmanczyk, M., 2011. Demonstration and validation of a 3d cfd simulation tool predicting pump performance and cavitation for industrial applications. *Journal of Fluids Engineering*, 133(1), pp.1-14.

Gopalan, S. and Katz, J., 2000. Flow structure and modeling issues in the closure region of attached cavitation. *Physics of Fluids*, 12(4), pp.895-911.

Hagar, A.E.D., Zhang, Y.S and Medhat, E., 2012. A computational study of cavitation model validity using a new quantitative criterion. *Chinese Physics Letters*, 29(6), pp.064703(1-3).

Hirschi, R., Favre, J.N., Parkinson, E., Guelich, J.F., Dupont, P. and Avellan, F., 1998. Centrifugal pump performance drop due to leading edge cavitation: numerical predictions compared with model tests. *ASME Journal of Fluids Engineering*, 120(4), pp.705-711.

Kunz, R.F., Boger, D.A., Stinebring, D.R., Chyczewski, T.S., Lindau, J.W., Gibeling, H.J., Venkateswaran, S. and Govindan, T.R., 2000. A preconditioned Navier-Stokes method for two-phase flows with application to cavitation prediction. *Computers and Fluids*, 29(8), pp.849-875.

Lei, T., Shu-Liang, C., Yu-Ming, W. and Bao-Shan, Z., 2012. Numerical simulation of cavitation in a centrifugal pump at low flow rate. *Chinese Physics Letter,* 29(1), pp.014702(1-4).

Liu, H.L., Ren, Y., Wang, K., Wu, D.H., Ru, W.M. and Tan, M.G., 2012. Research of inner floe in a double blades pump based on OPENFOAM. *Journal of Hydrodynamics*, 24(2), pp.226-234.

Liu, H.L., Wang, Y., Yuan, S.Q., Tan, M.G. and Wang, K., 2010. Effects of blade number on characteristics of centrifugal pumps. *Chinese Journal of Mechanical Engineering*, 23(6), pp.742-747.

Liu, H.L., Liu, D.X., Wang, Y., Wu, X.F. and Zhuang, S.G., 2012. Applicative evaluation of three cavitating models on cavitating flow calculation in centrifugal pump. *Transactions of the Chinese Society of Agricultural Engineering*, 28(16), pp.54-59.

Marina, O., 2008. *Numerical investigation on the cavitating flow in a waterjet pump*. Master's Thesis. Chalmers University of Technology, Goteborg Sweden.

Merkle, C.L., Feng, J. and Buelow, P.E.O., 1998. Computational modeling of the dynamics of sheet cavitation. *Proceedings of Third International Symposium on Cavitation*, Grenoble, France, 7-10 April 2008, pp.307-311.

Schiavello, B. and Visser, F.C., 2009. Pump cavitation-Various npshr criteria, npsha margins, and impeller life expectancy. *Proceedings of the twenty-fifth international pump users symposium*, Houston, USA, 23-26 February, pp.113-144.

Schnerr, G.H. and Sauer, J., 2001. Physical and numerical modeling of unsteady cavitation dynamics. *Proceedings of ICMF2001 International Conference on Multiphase Flow*, New Orleans, USA, 27 May-1 June, pp.1-8.

Senocak, I. and Shyy, W., 2002. Evaluation of cavitation models for Navier-Stokes computations. *Proceedings of the ASME2002 Fluids Engineering Division Summer Meeting Montreal (FEDSM '02)*, Quebec, Canada, 14-18 July 2002, pp.395-401.

Senocak, I. and Shyy, W., 2004. Interfacial dynamics-based modeling of turbulent cavitating flows, Part-1: Model development and steady-state computations. *International Journal for Numerical Method in Fluids*, 44(9), pp.975-995.

Singhal, A. K., Athavale, M. M., Li, H. and Jiang, Y., 2002. Mathematical basis and validation of the full cavitation model. *Journal of Fluids Engineering*, 124(3), pp.617-624.

Wang, Y., Liu, H. L., Yuan, S. Q., Tan, M. G. and Wang, K., 2011. CFD simulation on cavitation characteristics in centrifugal pump. *Journal of Drainage and Irrigation Machinery Engineering*, 29(2), pp.99-103.

Yang, M. G., Yin, B. X., Kang, C., Sun, X. K. and Che, Z. F., 2012. Numerical simulation of unsteady cavitating flow around hydrofoil. *Journal of Drainage and Irrigation Machinery Engineering*, 30(2), pp.192-197.

Zhou, L.J. and Wang, Z.W., 2008. Numerical simulation of cavitation around a hydrofoil and evaluation of a RNG k-ε model. *Journal of Fluids Engineering*, 130(1), pp.1-7.

Zwart, P., Gerber, A.G. and Belamri, T.A., 2004. A Two-phase flow model for predicting cavitation dynamics. *Proceedings of ICMF2004 International Conference on Multiphase Flow*, Yokohama, Japan, 30 May-3 June, pp.1-11.